

Servo-controlled Semi-rigid Exoskeleton Designed for the Human Knee

Runxing Kenneth Fu

Chinese International School, Hong Kong

ABSTRACT

Musculoskeletal injuries are occurring more and more frequently, with one of the main causes being the increasing number of new patients who sustain knee structure injuries. Currently, exoskeletons that assist the knee joint are either fully rigid or soft systems, which induce the risk of misalignments due to the complicated nature of the kinematics of the knee joint or require additional anchors or mechanical parts that may cause discomfort or force unnecessary weight upon the user. In this paper, a semi-rigid exoskeleton principle is introduced. This exoskeleton addresses the concerns of both rigid and soft exoskeletons while performing the same benefits by establishing a pre-determined route for the tendon. This exoskeleton can provide up to 37.26Nm assistive torque to the knee joint. The system's effectiveness was validated through a series of experiments which included testing its range of motion, total tensile force, and accuracy and safety of the pose detection system. The prototype had successful results, and the overall system is efficient, flexible, and easy to use. Future work will focus more on a customizable system in which the users can determine the amount of assistive torque force they need to be applied to their knee joint depending on their current physical ability.

Introduction

Throughout the past few decades, human exoskeletons, first invented in the 1960s, are being used much more frequently in medical, military, manufacturing, and industrial application fields. An exoskeleton is essentially an external frame that is worn on the body and can be used to help overcome injuries or enhance biological capacities. They are often powered by electric motors and allow users to develop extra movement, strength, or endurance.

These exoskeletons help disabled or injured people perform day-to-day tasks more effectively and efficiently or reduce the risk of injuries such as ones involving heavy loads by transferring the force onto the exoskeleton frame.

Kinematics of the Knee Joint

The human knee is actually one of the most complicated and intricate joints within our body as must be mobile enough to allow a dynamic range of motion, yet also must maintain stability when it is fully stretched. The knee joint is largely comprised of one principal Degree of Freedom, the flexion and extension one that can be modeled by the Knee Flexion Angle (KFA). According to [2], the KFA can reach up to a maximum of 140 degrees when in full voluntary motion, while roughly 160 degrees can be reached during passive motion.

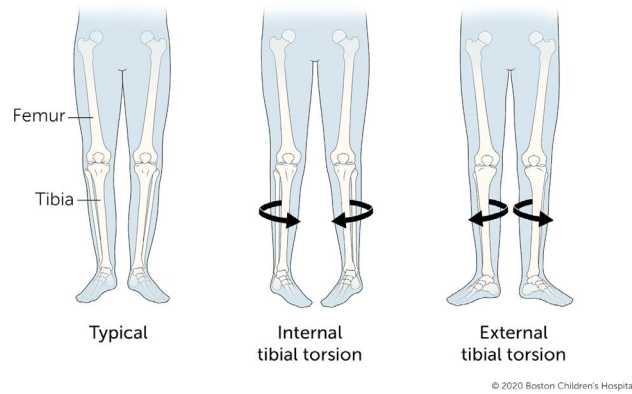


Figure 1: Tibia rotation [3]

In addition, as the articulating surface around the knee joint is relatively complex, human biological geometry actually changes the center of rotation of our joints, namely internal and external tibia rotation when the knee joint is flexed. This is the twisting of the shinbone (tibia), and can be defined as the rotation angle of the sagittal plane through the rotation axis. For example, when the KFA is 90 degrees, the internal tibia rotation is 30 and 35 degrees during voluntary and passive motion respectively. On the other hand, the external tibia rotation is 40 and 50 degrees during voluntary and passive motion respectively. Furthermore, [2] denotes that when the knee is fully extended during each gait cycle, a natural external shank rotation occurs to the knee joint, while an internal shank rotation occurs when the knee joint is flexed. Lastly, as the KFA is changing/when the knee joint is being flexed or extended, the instantaneous center of rotation of the knee joint actually shifts roughly 2 centimeters along the sagittal or longitudinal plane.

Related Literature

The benefits of exoskeletons upon so many facets of human health and development have interested many researchers in the past, and many have designed their own exoskeletons in an effort to reap such benefits.

One such exoskeleton found in the *International Journal of Humanoid Robotics* designed by three researchers denotes a quasi-passive exoskeleton intended to alleviate stress from the lower body when carrying additional weight while walking. Their exoskeleton (figure 2b) uses ankle and hip springs, a knee variable damper, and no actuators in order to transfer the weight carried onto the ground, thereby reducing the force exerted upon the body.

However, the knee variable damper executed on this exoskeleton represents the knee joint as a single degree of freedom, which is susceptible to many aforementioned problems regarding the misalignments between the flexion and extension axis of rotation of the exoskeleton and of the knee joint. Therefore, the misalignment issues caused by many such exoskeletons can cause discomfort to and potentially harm users in worst-case scenarios. To combat this problem, new types of exoskeletons were introduced which can be classified as rigid and soft exoskeletons.

[1] proposed a solution to this problem that requires at least 5 more degrees of freedom, which would all work to accommodate the one main active degree of freedom. Many rigid devices, such as the iT-Knee, adopted this solution and incorporated additional degrees of freedom in order to compensate for the slight rotations and changes along the sagittal plane.

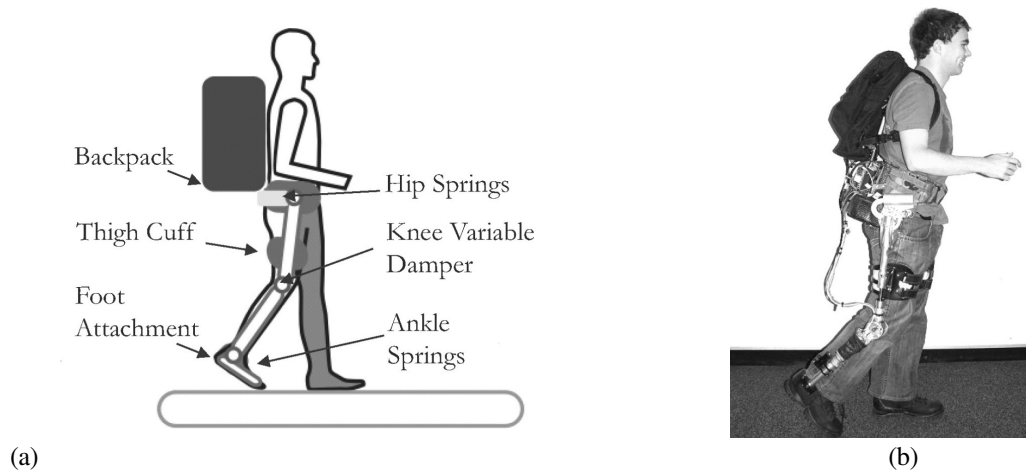


Figure 2: Prototype of quasi-passive leg exoskeleton: (a) annotated graphic design, (b) prototype tested on human [2]

The iT-Knee [3], developed by three researchers in 2016, makes use of six degrees of freedom in order to deliver pure torque assistance to the knee joint, with one active degree of freedom and five passive ones for self-aligning purposes. Although the iT-Knee and similar rigid exoskeletons are able to compensate for the knee joint's unique movement and perform more accurately, many of these additional degrees of freedom are quite redundant and force the system to become heavier and less convenient.

On the other hand, soft exoskeletons such as one designed by Wehner et al. [4] are much lighter in weight compared to the aforementioned rigid exoskeletons and are primarily designed for gait assistance. Such exoskeletons are able to negate misalignment issues due to their inherent elasticity. However, this usually also requires an anchor on the human body or clothes, thereby possibly producing extra weight upon certain affected human joints and inducing discomfort or pain upon those joints.

As both rigid and soft exoskeleton systems have their own respective advantages and disadvantages, this project proposes a novel approach for an exoskeleton targeted toward the knee joint which addresses the concerns listed above in relation to the rigid and soft exoskeleton structures while delivering all the same benefits to a similar extent. The proposed system seeks to enhance overall performance and strength for users suffering from knee injuries or pains by lessening the force exerted upon the knee joint when performing physiotherapeutic or general exercises and procedures.

The report is organized as follows: Section II describes the theoretical design of the proposed exoskeleton, and denotes the initial formulas and structure. Section III presents the actuation and final design of each part presented in section II as well as any changes proposed. Section IV presents the electronics and code used to allow the exoskeleton to properly perform upon a human. Section V introduces the experiments performed and the results collected. Lastly, section VI presents my future expectations for the exoskeleton and concludes the paper.

Theoretical design

Routing System:

The guiding route is one of the main features of the exoskeleton design which starts from the thigh and is extended down towards the calf. A semi-rigid chain will follow along this route to ensure the transmission tendon of the system is able to pass the knee joint without any aforementioned concerns about misalignment or interference is-

sues. The parameters of the guiding route are incorporated so that the chain won't interfere with the range of the knee's movement, and is also compatible with different body sizes. Therefore, the guiding route of the chain mechanism is comprised of a circle and an ellipse with the parameters indicated below,

where x_c and y_c represent the starting cartesian coordinates of the circle while x_e and y_e represent the starting cartesian coordinates of the ellipse. r represents the radius of the circle and a and b represent the ellipse's two axes.

Circle			Ellipse			
x_c	y_c	r	x_e	y_e	a	b
0.110	-0.080	0.090	0.125	-0.015	0.125	0.165

As a whole, the merging point between the circle and ellipse is at (-0.033, 0.127), so the entire function of the guiding route can be expressed as $f(x)$ below.

$$f(x) = \begin{cases} 0.165 \sqrt{1 - \frac{(x+0.125)^2}{0.125^2}} + 0.01 & -0.033 < x \leq 0 \\ \sqrt{0.09^2 - (x + 0.11)^2} + 0.08 & -0.071 \leq x \leq -0.033 \end{cases}$$

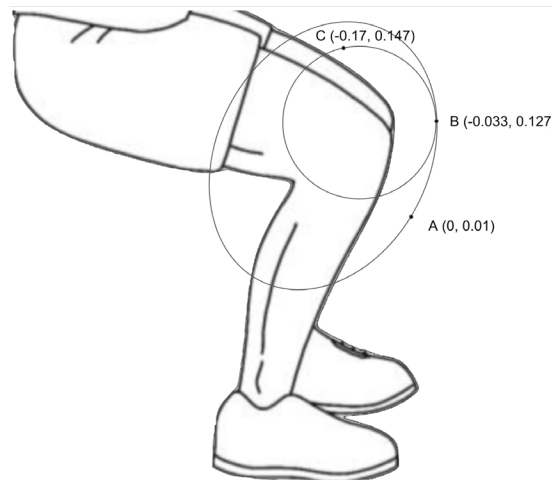


Figure 3: The routing system structure concept at 100° KFA

As shown in figure 3, there are three important points, A, B, and C, respectively colored yellow, red, and blue on the guiding route. The coordinates of these points are A(0, 0.01), B(-0.033, 0.127) and C(-0.17, 0.147). Point A represents the start of the chain mechanism, point B represents the aforementioned intersection and transition point between the circle and ellipse, and point C represents the end of the chain mechanism. As demonstrated by the figure, even during extremely acute knee flexion angles, the semi-rigid design of the mechanism is able to ensure that no external force is applied to the tissue around the knee joint. Furthermore, it creates a predetermined route for the chaining such that the values determined by the system software design/algorithm can accurately determine the angle of tilt without any misalignments.

Structural Design

Outer Shell System:

In the design of the routing system, the overall design follows the constraints denoted above regarding the combination of a circle and ellipse to imitate a real person's leg. Building on this foundation, it can be seen from Figure 4 that the routing system is split into 5 separate components.

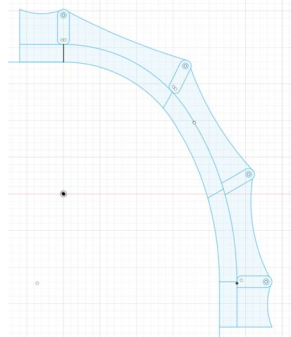


Figure 4: 2D model of routing system

One main benefit of changing this routing system into 5 different segments is the additional flexibility that is allowed. As a human's leg and knee flexion angle will frequently change when in motion, this design allows the exoskeleton to become more flexible and adaptable to the person's movement, as well as being more comfortable and natural to the user. For a more ergonomic design, all the corners and straight edges have also been curved in order to minimize any physical harm upon physical contact.

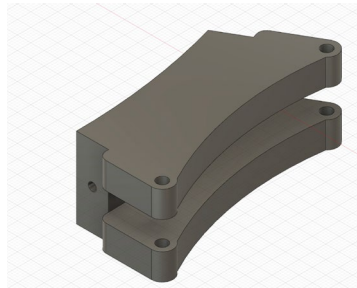


Figure 5: 3D model of a segment of the routing system

Figure 5 is an example of one of the five segments. I cut out the top half's middle part so that the adjacent segments would be able to fit into the gap and be connected using the holes on either side. Therefore, an alternating pattern was designed in which they would be able to smoothly connect to each other while maintaining the routing system shape. The bottom half (uncut side) of each segment mimics the routing route pattern and is uncut so that the exoskeleton has a basic foundational shape. The holes used to connect the adjacent segments together are placed on the edges of the segment as this ensures maximum flexibility and rotational ability. The exoskeleton will also be able to adjust according to people with different heights and sizes, as the semi-rigid structure allows for compatibility for different users.

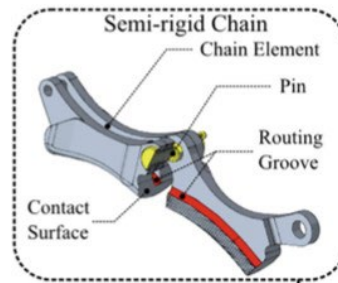


Figure 6: Semi-rigid chain diagram

As seen from figure 6, these 5 segments can be defined as modular-designed semi-rigid chains which consist of chain elements, pins, routing grooves, and contact surfaces. The routing groove from each semi-rigid chain shown above is what will be used to implement the aforementioned routing system suited to the human anatomy, and it will be the base of each chain. To ensure that the metallic string is able to follow the routing system, a hole is placed along the routing groove so that the string is able to not only follow the predetermined guiding route but will also be secure throughout the entire exoskeleton. As seen in figure 6, the pin is designed optimally for flexibility and allows for each semi-rigid chain to rotate individually modularly as a human's leg's motion is not completely uniform until it is along the routing groove. The design of the pin and chains also allows for secure stability, as the dimensions of each chain are adjusted such that they just perfectly can fit into each other, and can be easily secured by the pin. As aforementioned, the contact surface of each chain is also smoothed out so that there aren't any sharp corners or anything that could cause potential harm.

First Design:

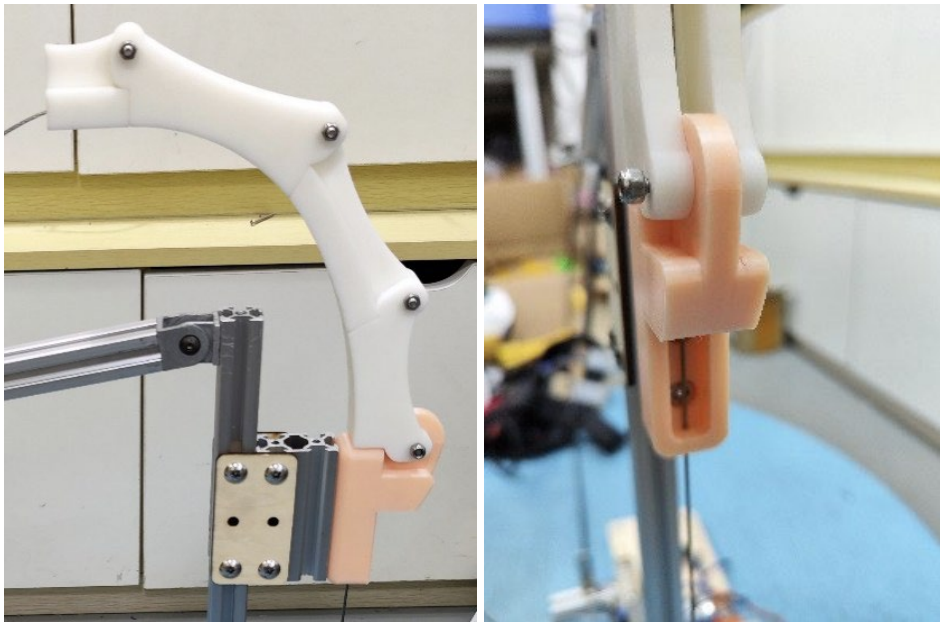


Figure 7: 3D printed model of outer shell system

The outer shell was first created using 3D printed plastic, as a 3D printer allows the product to be made faster, thus making the overall planning and materializing process much faster. However, the 3D printed plastic is also extremely weak in comparison to sturdier materials such as metals. Thus, the system can easily break under high amounts of pressure or force, meaning it will not be able to provide the necessary levels of assistive torque to the knee joint.

Final Design:

To counteract the weakness of the 3D-printed plastic, the material of the outer shell was replaced with steel, which can withstand significantly higher levels of force. However, as steel products are much harder to manufacture in comparison to 3D-printed products, the exact structure of the outer shell was modified into a simpler one while still maintaining the routing system and the flexibility of the 5 segments.

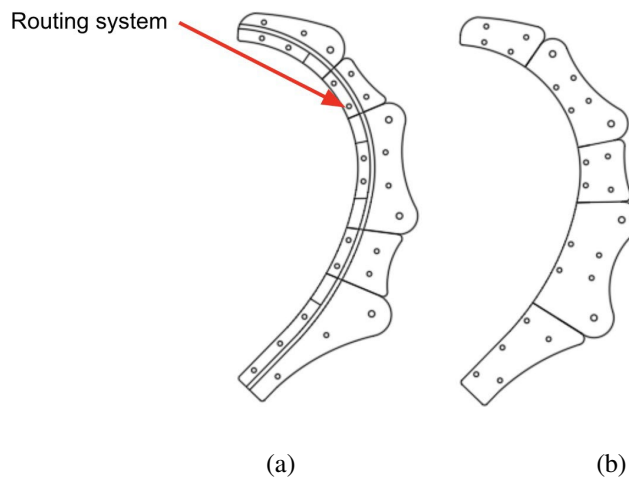


Figure 8: 2D model of new outer shell structure (a) inside, (b) outside

As seen from figure 8, the new structure is much simpler overall while maintaining the correct routing system. This improvement means that it can be made in adequate time while also improving the overall solidity of the structure.

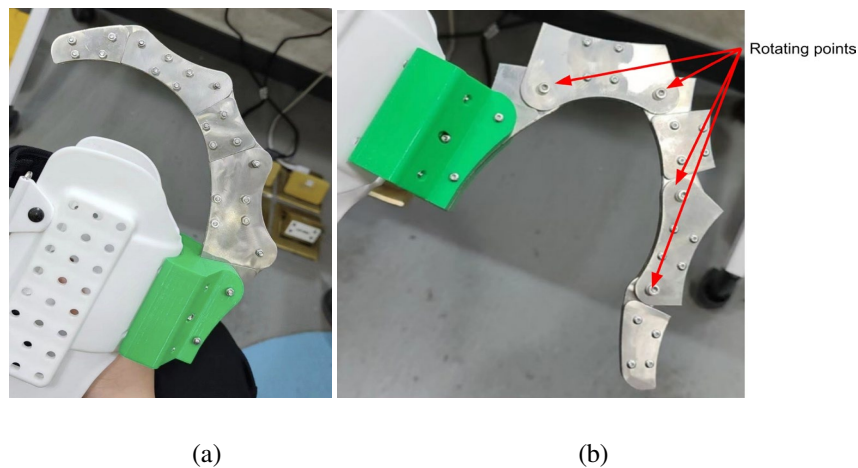


Figure 9: Physical model of new outer shell structure

From figure 9, it can be seen that the 5 segments are connected together with the use of stop bolts and locknuts in order to secure them tightly together. The stop bolts and locknuts work together to reduce the force of friction acting on the system, while also ensuring stability throughout, meaning the segments are able to flex smoothly according to the user's movements. In figure 9b, the rotating points between each of the 5 segments are pointed out, and this is achieved using joints that can be rotated.

Shin Pad:

As the routing system must be connected to the shin pad that helps support the entire exoskeleton, I specially modified the last segment of the routing system's outer shell (the bottom one) so that it would be easily attachable to the shin pad.

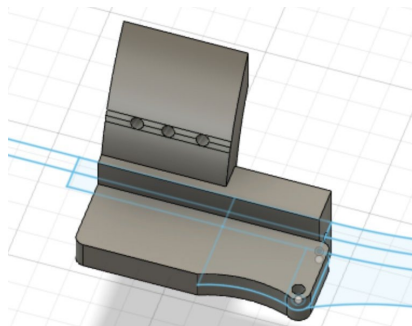


Figure 10: Attachment to shin pad

As the shin pad is slightly curved to suit the shape of a leg, I added a flap to both sides of this segment as seen in the image above with three holes in the middle so that they would be able to connect with the holes on the shin pad. The three holes allow the user to adjust the exoskeleton based on their height/body size.

Waist Harness Attachment:

First Design:

The routing system must also be connected to a harness attached to the user's waist in order to hold the system up, and this is where the servo used to provide strength will be located.

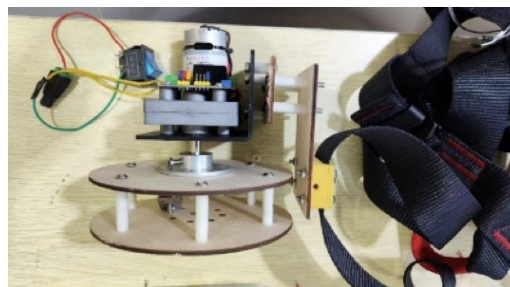


Figure 11: Top-down view of the servo attached to the waist harness

As seen from figure 11, the initial design of the attachment connects the harness together with the servo through the use of a basic 3D printed attachment that fastens the two together with a screw.

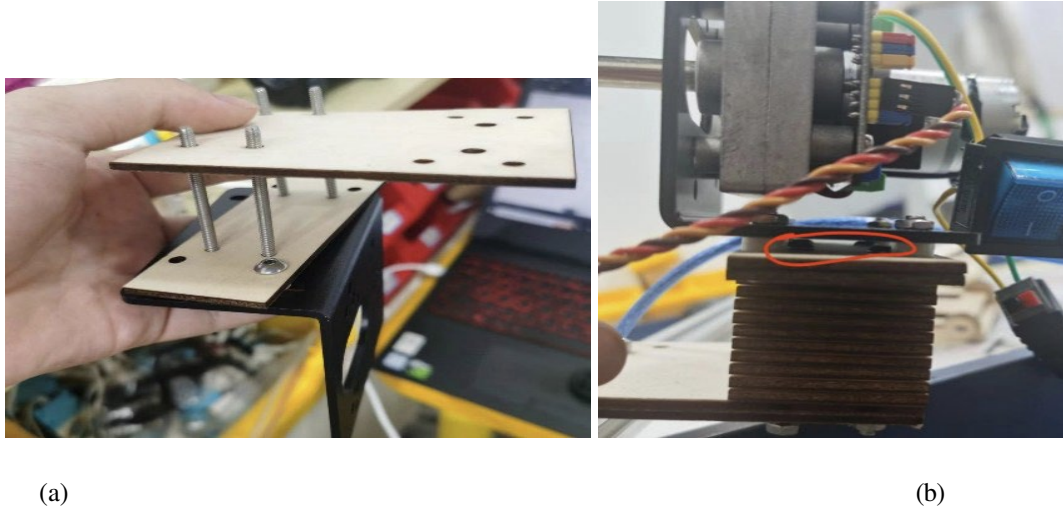


Figure 12: Separation distance between the servo and harness

However, as seen from figure 12, the distance between the servo and harness is quite significant in this design and had to be accounted for using small plastic placeholders as seen in figure 11. This is due to the size of the reel, as the reel is significantly larger than the servo, meaning extra space had to be added so that the reel wouldn't collide with the harness or user. Therefore, the overall structure of the system is much looser and weaker and is much more susceptible to being damaged or changing form while in use, leading to a much shorter overall life span.

Second Design:

During initial experimental testing of the system from the first design, it was found that the size of the reel doesn't have too significant of an impact on the overall performance of the system. Therefore, to make up for the downsides deduced from the first design, the overall size of the reel was significantly reduced so that it is roughly proportional to the size of the servo.

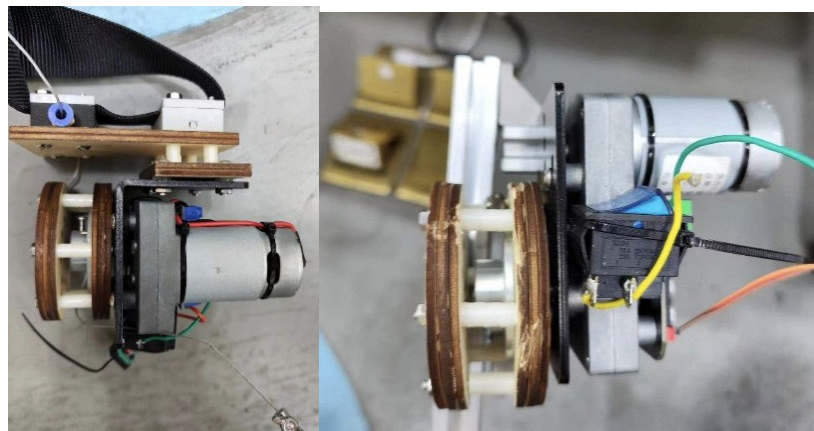
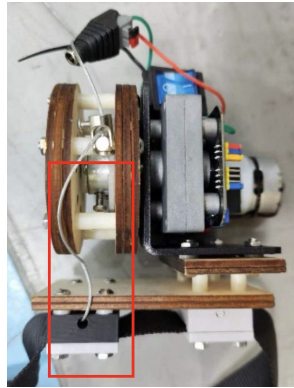


Figure 13: Top-down view of the second waist harness attachment design

As seen from figure 13, the reduced size of the reel allows for a much shorter distance between the harness and the servo, as the size of the reel does not have to be accounted for anymore. This creates a much more compact design overall that is tighter and more secure, accounting for the problems of changing shape or being easily damaged from the first design.

Figure 14: Annotated image of second design



However, one major problem outlined in figure 14 is the pathing of the metallic cord, as the cord must be turned upside down at a high angle in order to enter the reel. Not only is this severely inconvenient and awkward for the user and system, but through experimental testing, it was also found that when there's a relatively high torque force generated at the knee joint, the friction force exerted upon the wooden board is also at a high volume. This friction makes it difficult for the reel to be able to pull on the metallic cord, and if the system is used at a high volume, the friction will also damage the wooden board, potentially causing a shorter life span and a weaker overall system.

Final Design:

The final design of the waist harness attachment ensures a system that resolves the problems found in the first and second designs and also creates a much more secure, concise, and user-friendly system.

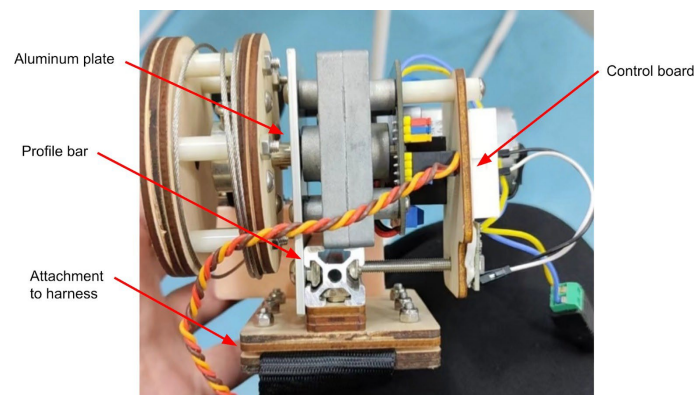


Figure 15: Annotated image of final design

Firstly, as seen in figure 15, the overall structure and materials used in the system have been modified to enhance the overall solidity of the design. An aluminum plate together with a profile bar is used to connect the reel with the servo, which will then be connected to the harness. As seen in figure 13, the previous installment con-

nected the servo and reel to a wooden board, which was then connected to another board a small distance away, and finally connected to the harness using 3D-printed attachments. This design of the structure removes the unnecessary parts used to connect the harness with the servo and reel by directly attaching them together with four wooden boards, in which two wooden boards stand on either side of the harness strap, and are tightly secured together with screws. This simplified structure not only minimizes the space required for the system but the new materials and attachments ensure a significantly sturdier overall structure. Furthermore, the control board used for the electronics part of the system is attached on top of the servo without taking much extra space, thereby further reducing the space required to maximize the efficiency and ergonomics of the design.

The use of the four wooden boards to connect the harness strap with the servo also allows changes to the positions of any part easier to make. In the previous two iterations, the entire system must be taken apart in order to make any changes or adjustments necessary. However, in this design, once the screws connecting the four wooden boards together are loosened, the structure can immediately be adjusted.

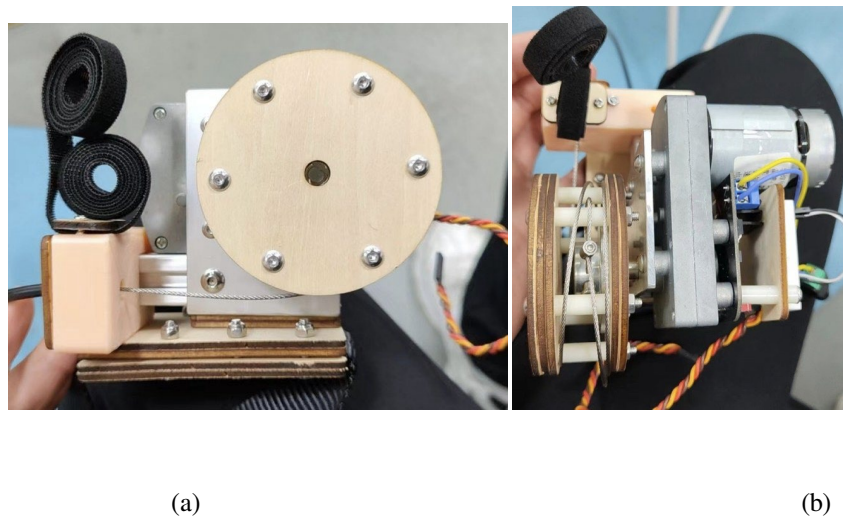


Figure 16: Final design (a) side view, (b) top-down view

To address the problem of the metallic cord's pathing from the second design, a 3D-printed attachment was added as seen in figure 16. This attachment secures an opening and routing path for the metallic cord so that it can connect with the reel in a direct line without awkward turns, thus minimizing the space required for the routing path of the metallic cord and making the overall design more concise and convenient for the user.

Another problem found with the design is the effect of gravity upon the system, as the weight of the servo often causes the parts to lean and fall downwards. Therefore, as seen in figure 16, a velcro was installed that can be directly connected to the upper body, which will negate the downward motion from the effect of gravity upon the system.

Elastic Element

In the drivetrain, an elastic element is used that enables impact absorption and also can reduce the influence of weight, or passive load compensation. This elastic element is attached around the calf area and is connected to the routing system around the knee.

For this system, as the tension force required to support the generated torque force from the knee is relatively high, an elastic element that can support a high tension force is required. Therefore, a bungee cord was chosen, as they are extremely efficient at lifting, moving, or lowering heavy items.

Material Attachments

3D Printed Plastic

The majority of shapes and designs assembled are 3D printed using plastic, as this is an abundant material that is both cheap and convenient to create. The designs on some parts are also quite intricate, meaning it would be much easier first to assemble using a 3D printer with plastic.

However, for the actuation of the final exoskeleton, parts of the 3D-printed plastic such as the outer shell of the routing system will likely be changed into metal, a much sturdier material, as it is hard for plastic to be able to support a human's weight.

Metallic Stand

The stand used to upright the exoskeleton and help conduct the experiments is metallic since metal is stronger and heavier, meaning the base can support more weight and the entire exoskeleton while performing experiments. Furthermore, the stand is largely comprised of very basic shapes, meaning it isn't necessary to 3D print the stand.

Electronics

Sensors

The exoskeleton uses two inertial measurement units (IMUs) in the form of mpu6050s, which is a Micro Electro-mechanical system (MEMS) that consists of a three-axis accelerometer and three-axis gyroscope. It helps us to measure velocity, orientation, acceleration, displacement, and other motion-like features. The accelerometer is used in the mpu6050 to determine the acceleration due to movement and also acceleration due to gravity. Normally an accelerometer's x and y output voltages will be half the supply voltage when measuring zero g (i.e. the device is perpendicular to gravity - horizontal). Tilt it one way and the voltage will increase, tilt it the other way and it will decrease. With a Triple axis accelerometer, the z-axis will be measuring 1g with the device horizontal. The output of an accelerometer is a sinewave of the acceleration measured.

The inclination sensing used in this project uses the gravity vector and its projection upon the accelerometer's axes to find the angle of tilt. As the human leg will induce a centripetal acceleration upon the accelerometer and rotate, the output will also change accordingly as gravity is a DC acceleration.

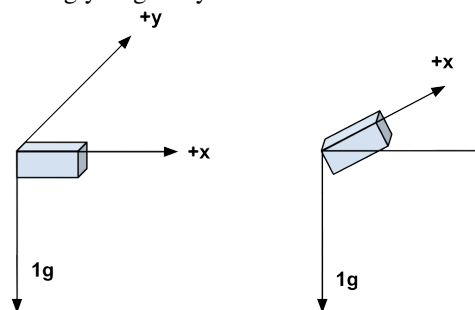


Figure 17: Diagram for tilt sensing using accelerometer

As seen from Figure 17, the angle of tilt can be determined through the accelerometer's variable X as we are only measuring a relatively limited angle that can be measured by a single axis. Using the diagram above, we can

infer using basic trigonometry that the output acceleration produced by the projection of the gravity vector is equal to sine theta, the angle between the accelerometer x-axis and the horizontal, which is perpendicular to the gravity vector. Taking gravity to be equal to 1g, the output acceleration can be expressed as:

$$A = g \times \sin(\theta). \quad (1)$$

Rearranging (1) to find the inclination angle, θ , using the acceleration determined from the accelerometer, we get:

$$\theta = \sin^{-1}\left(\frac{A}{g}\right) \quad (2)$$

where the inclination angle is in radians. To change the value of θ back into degrees, we can multiply θ by $\frac{180}{\pi}$ to find the inclination angle in degrees.

Servo

The servo chosen for this system is the DH-03X. Originally, the model chosen could provide a maximum torque of 180kgf cm. However, after experimenting with the estimated torque generated by the human knee joint, the torque provided by this servo wouldn't be able to satisfy that of the human knee. Therefore, the servo was upgraded to the model that can provide a maximum torque of 380kgf cm. Therefore, after converting this value into Newton-meter form, this system will be able to provide up to 37.26Nm assistive torque to the knee joint.

Circuit Board

The circuit board used in this design is the Arduino UNO.

Data Processing and Decision Making

The data received from the two IMUs are transmitted to the Arduino Uno board and then processed through the implemented algorithm. The data processing is the aforementioned task of translating the accelerometer's variable X into a degree.

Servo Response

The servo is powered by a 24V battery that will initialize to 0 degrees with an on/off switch and will rotate to the desired position determined by the algorithm at a speed of 2 degrees every 80 milliseconds.

System Software Design

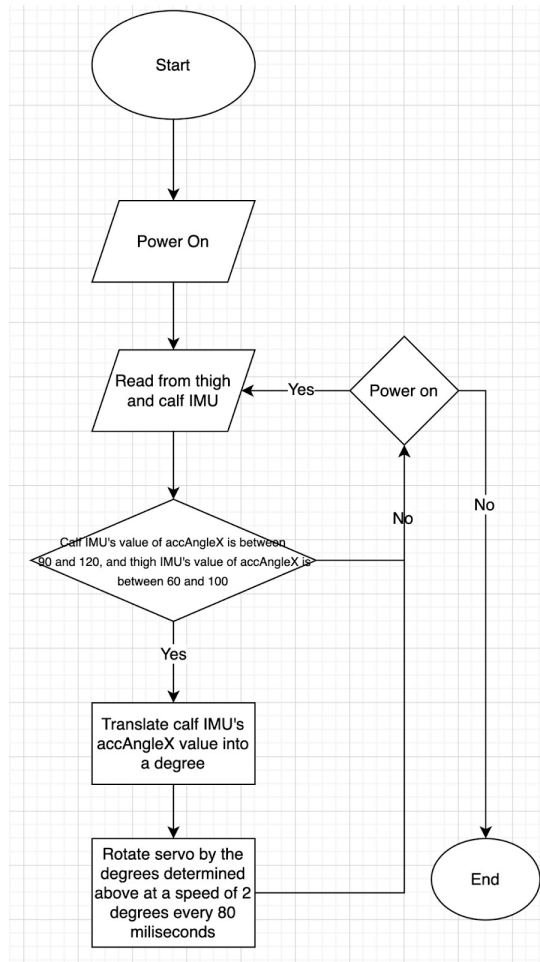


Figure 18: Working process of the whole program

The algorithm and software design of the system is shown in figure 18. The variable accAngleX represents the accelerometer’s variable X, which will then be used to determine the angle of tilt using the formula listed above.

Pose Detection

Another method used to determine the KFA is through the use of a machine learning solution that can predict and determine the locations of regions of interest, which are the key body parts in this case.

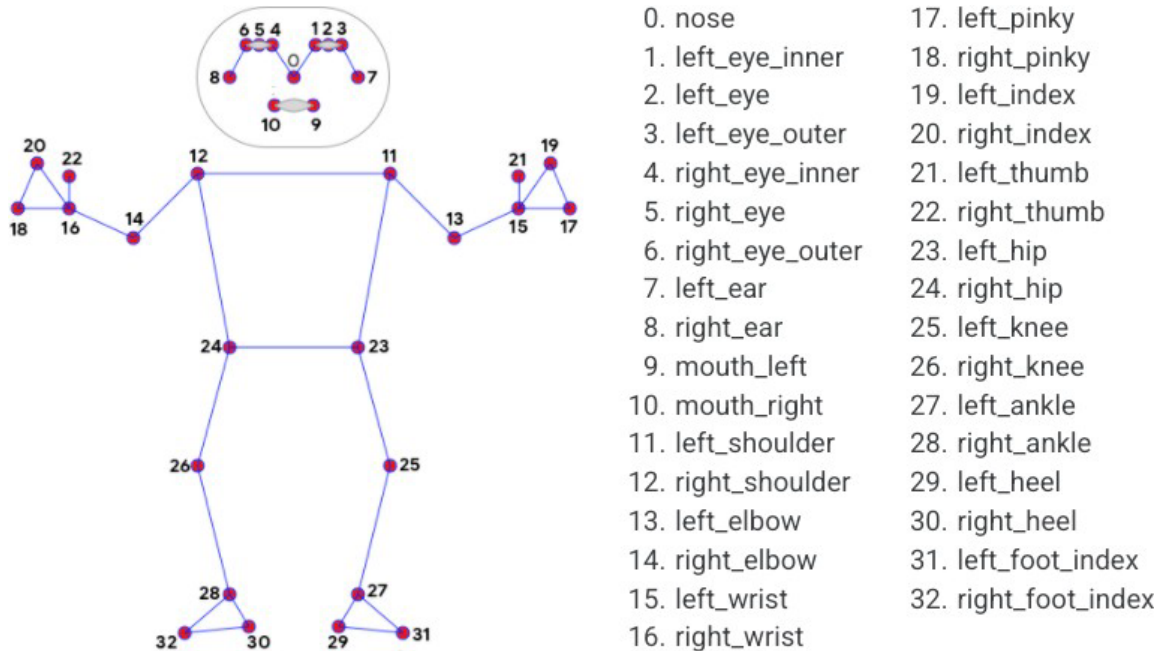


Figure 19: 33 pose landmarks [5]

Mediapipe offers a solution in which it is able to determine 33 particular regions of interest, outlined in figure 19. An algorithm was designed to rotate the servo depending on the current KFA through the medium of mediapipe to help calculate the KFA. As mediapipe allows us to determine the exact coordinates of the joints in the lower limb, the algorithm uses the positions of the right hip (24), right knee (26), and right ankle (28) to determine the KFA using the cosine formula. The chosen landmarks can be similarly replaced with the left hip, left knee, and left ankle. Additionally, mediapipe also determines the visibility of each joint, which is a quantified value for how clear it is able to see and determine each given landmark. Therefore, the algorithm will also note when the visibility of the three chosen landmarks is too low to safely change the torque force applied without potentially hurting the user.

Although the pose detection requires slightly more setup as a camera is required, the overall benefits compared to the IMU sensor far outweigh the extra amount of setup. Firstly, the accuracy of the machine learning algorithm is more accurate than the IMU sensors, as the sensors could potentially be affected by various different factors or unexpected movement, hence why two IMU sensors were required in the initial design to help cross-validate.

More importantly, as the goal of the system is to assist users while performing physiotherapeutic or regular exercises, the pose detection also allows users to better perform certain exercises. As seen from figure 20, the algorithm can determine the KFA at various different angles, and will print the current KFA on the screen. Therefore, as many rehabilitation processes such as [7] require the KFA to reach a certain degree, this system also allows the user to accurately determine their current KFA so that they can follow medical or physiotherapeutic procedures to a high degree.

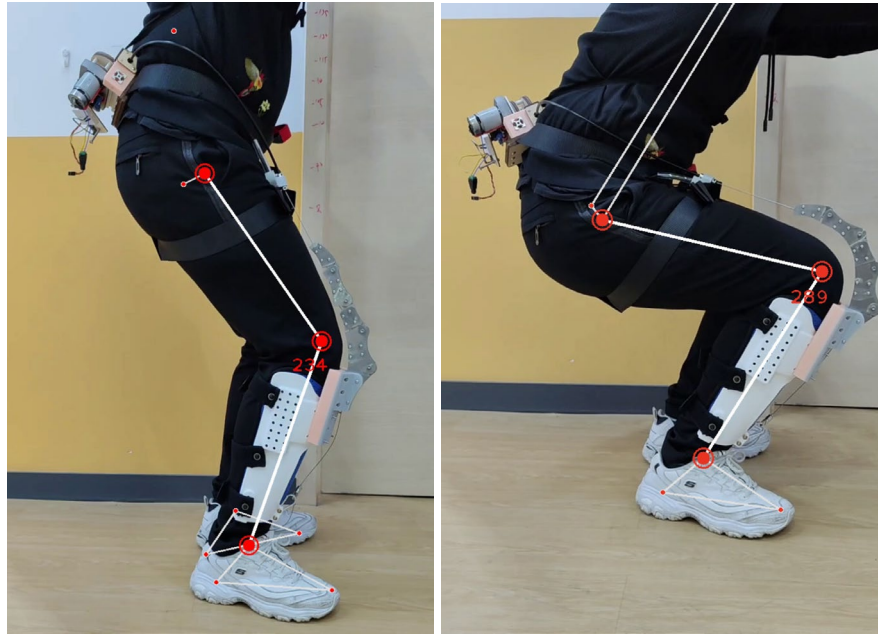


Figure 20: Knee flexion angle determined with algorithm

However, one downside to this method is the space required to setup the entire system. Firstly, for this algorithm to work, the camera must be placed pointing towards the right side of the user, so that it can accurately determine the positions of the right hip, right knee, and right ankle. If the camera is placed facing other directions, the visibility determined by the system won't be high enough to safely rotate the servo and provide assistive torque. Additionally, the camera must also be placed far away enough such that the entire lower body can be seen on camera, or the system won't be able to accurately calculate the KFA. Therefore, if users are operating in an extremely tight area, it is recommended to use the IMU sensors instead as they don't require any additional space. However, for the majority of users, the machine learning technique as aforementioned is significantly more efficient and accurate, and if they are able to fit the right hip, knee, and ankle within frame, then this procedure is recommended.

Circuit Board

To process the data using the pose detection method, two ESP32 boards are used instead of the Arduino board. One ESP32 board will be connected to the computer that has the pose detection and camera running, while the other board will be attached to the exoskeleton and connected to the servo. The board connected to the computer will first read the knee flexion angle calculated by the algorithm and will send the data to the other board through the wifi, as these boards are installed with a micro wifi chip. The board connected to the exoskeleton will then process the data and rotate the servo accordingly. The use of these ESP32 boards is much more effective as the two boards aren't directly connected to one another, meaning the user doesn't have to stand right next to the computer in order for the system to work, they just need to be close enough to be visible to the pose detection algorithm.

Experimental Validation

Experimental Setup

To ensure the safety of the user, while the exoskeleton is being used on the user's body, the metallic string will remain relaxed throughout, and there will be no force from the reel or the servo. Additionally, the movement of the human joints will be simulated using a setup to determine the experimental results.

Initial Setup:

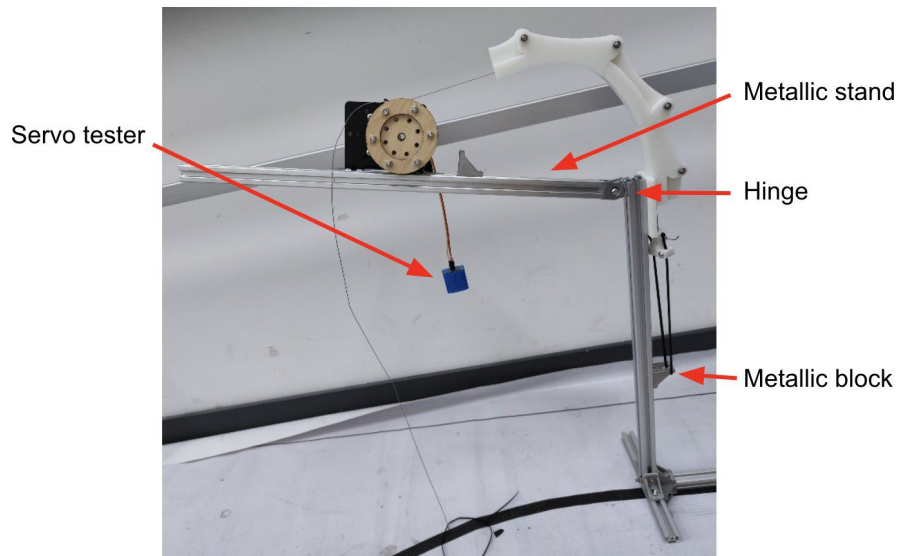


Figure 21: Initial experimental setup

As seen from figure 21, the initial experimental setup comprises the core elements of the system, which include the servo, reel, outer shell, metallic string, and an elastic element. As aforementioned, in consideration of the experimenting user, a metallic stand is used in place of the human lower body, where a hinge that can turn vertically is used to mimic the human knee joint. As the lower extremities are no longer required, the shin pad is also disregarded in this setup as we don't need to connect the elastic element with the lower body. Instead, a metallic block that is fixed to the stand is used to replicate the connection to the shin, and the elastic element is looped through the metallic block so that the system can function just as normal.

Lastly, a servo tester is used to control the motions of the servo and reel, so that during the experiments it can be tested how much load the system is able to carry up and down independently.

However, as the servo and reel are set up directly on the metallic stand and are hanging off one edge, this disrupts the system's center of gravity, meaning it is slowly twisting and falling off one side of the stand. If the servo falls too far off the stand, this could potentially damage the entire system, and will also significantly alter experimental results.

Second setup:

Figure 22: Second experimental setup

To fix the problem identified from the first experimental setup, the positioning of the servo and reel has been fixed onto the center of the metallic stand so that the center of gravity maintains in the middle. However, just fixing the servo and motor to the center alone creates an imbalance of force exerted on the metallic stand, so as seen from figure 22, the routing of the metallic cord is slightly more fixed using additional tools so that the imbalance is relatively marginal and negligible.

However, while the system is being used, the exact position of the servo is constantly changing, meaning this setup isn't an accurate representation of the real system. In the real system, the servo is directly connected and fixed to the waist harness, meaning that it won't be moving around. Therefore, any experimental results obtained using this setup could be skewed and regarded as invalid, thus requiring further modifications to the overall experimental setup.

Final Setup:

Another problem identified from the first two setups is the exact positioning of the routing system in relation to the knee joint (the hinge on the metallic stand). In the theoretical design of the routing system, the center of both the circle and ellipse is the knee joint, as the system must wrap around the knee and leg area. However, from figures 19 and 20, it is evident that the routing system does not match the theoretical design and is situated much higher than it should be. This problem was addressed in the final experimental setup.



Figure 23: Final experimental setup

In figure 23, it can be seen that the routing system has been lowered using a metallic block which is fixed onto the metallic stand using screws and two wooden boards, thereby adjusting the center of the routing system's design to the knee joint. Furthermore, the issues of the placement of the servo and reel from both setups 1 and 2 have also been addressed. As placing the servo on the metallic stand would cause various issues regarding instability or unexpected change of positioning, the final experimental setup shown in figure 23 relocates the servo and reel to the base of the stand. By relocating the control parts to the bottom of the stand, the overall experimenting process was also able to be expedited and made more realistic through two methods.

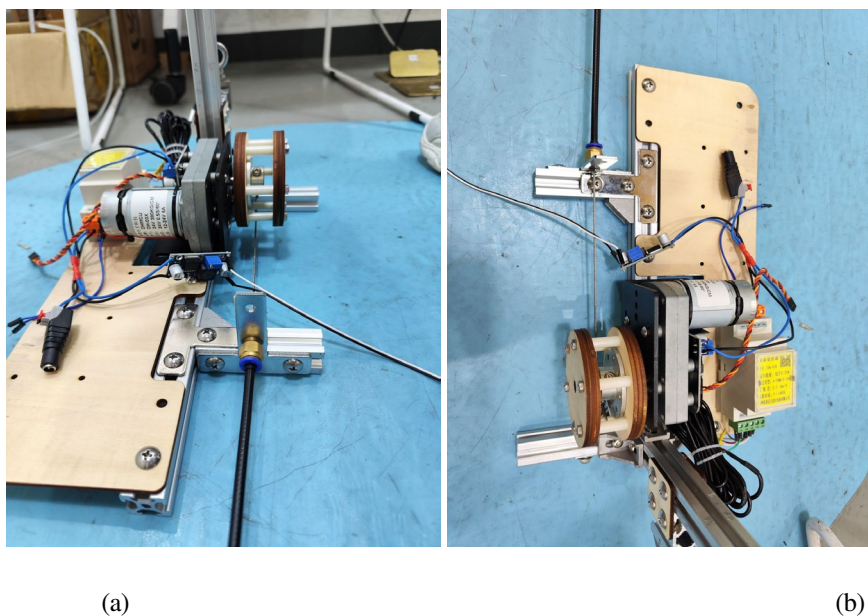


Figure 24: Base of the setup

Firstly, as seen in figure 24, the pathing of the metallic cord is perfectly straight as it reaches the reel, meaning the system is working with maximum effectiveness and is able to perform similarly to how it would on a human body. From figure 22, the pathing of the cord from the routing system all the way to the servo is also extremely simple, concise, and elegant, as it follows a circular path that doesn't include any sharp turns.

Secondly, by relocating all the control objects and motors to the base of the system, more space can be used here, and additions can be added to supplement the experimenting process. In figure 24, a tension sensor was added next to the servo. This addition allows experiments involving the tension force of the rope much easier to conduct, thereby expediting the overall experimental process, and enhancing the results obtained.

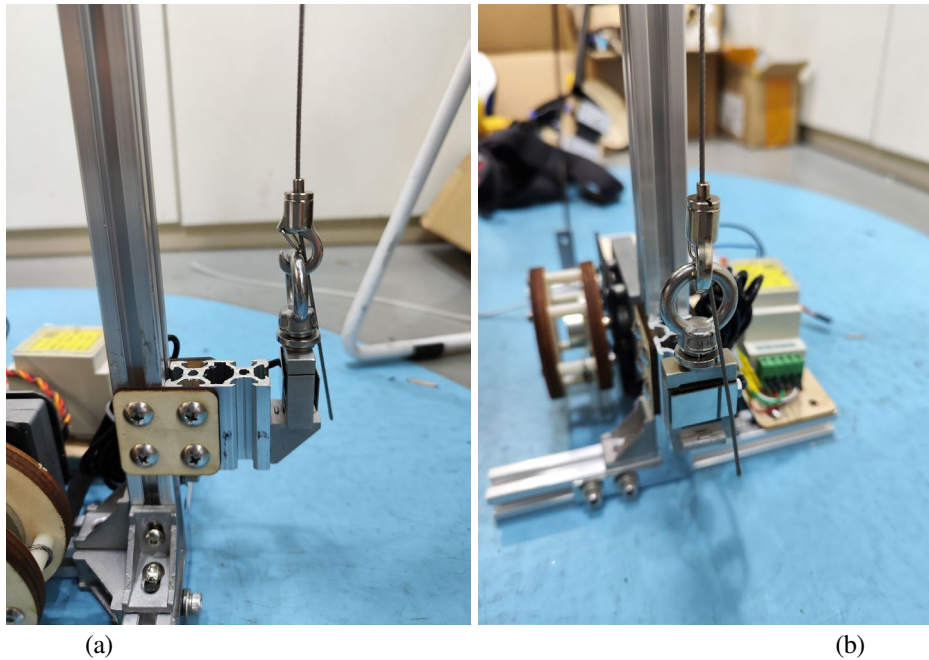


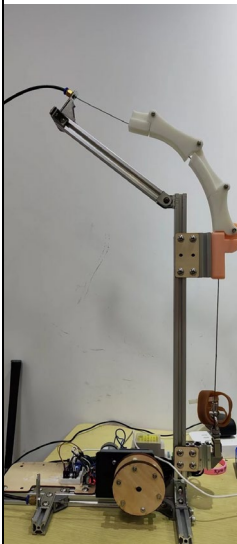
Figure 25: Addition of turnbuckle

Additionally, a turnbuckle was added to connect the bungee cord with the makeshift shinpad. Turnbuckles are extremely useful at adjusting the tension and length of ropes, which further elevates the system's ability to conduct a range of different experiments effectively and allows the user to easily adjust the starting height, length, or tension of the rope depending on the experiment.

Experiments

First experiment:

The first experiment investigates how much the knee flexion angle changes through a full rotation of the servo. Though the servo is able to rotate from 0 degrees up to 300 degrees, the knee flexion angle does not change at the same rate as the servo. Therefore, this experiment can help determine the range of motion in which the exoskeleton is able to deliver assistive torque to the knee joint. Two variables will be recorded in this experiment, in which the starting degree, also the largest degree, will be the independent variable, while the dependent variable is the smallest degree that can be reached. The difference in degrees will be calculated as the difference between the two variables. To conduct this experiment, the system designed in the aforementioned final experimental setup was placed on a flat table. No additional load was added to the system too, and the only weight that the exoskeleton would be applying force to would be the weight of the metallic stand.

Trial Number	Smallest degree	Largest degree	Difference in degrees	Image at smallest degree	Image at largest degree
1	36	118	82		
2	43	128	85		
3	55	144	89		
Average	44.7	130.0	85.3		

According to the results of the experiment trials, the average difference between the largest degree and the smallest degree is 85.3 degrees, meaning the system can support 85.3 degrees of rotation on average. In the regular squatting motion in which strength from the thigh is required, the angle is roughly between 45 and 125 degrees, which is a difference of 80 degrees, which fits well with the second trial from the experiment, and also fits within the 85.3 degrees of rotation that was calculated from the experiment. Therefore, the system is able to provide assistive torque throughout the user's entire squatting motion.

Second experiment:

The second experiment investigates the relationship between the analog value and the tensile force. My hypothesis is that the analog value and the tensile force are directly proportional and that the analog value of 1023 should correspond to the tensile force value of 100kg.

In the setup of the experiment, a load cell with a capacity of up to 100kg is installed onto one end of the metallic cord, and the output of the load cell is connected to the control board which can then output an analog value between 0 and 1023 on the computer.



Figure 26: Experiment setup

As seen in figure 26, to conduct the experiment, a force gauge was attached to one end of the load cell. During the experiment, the force gauge would be pulled backward until its value reached 2kg, 4kg, 6kg, 8kg, and 10kg, and between each pull, it would be returned to equilibrium. This process was repeated six times, and the results were displayed in a graph format in figure 27.

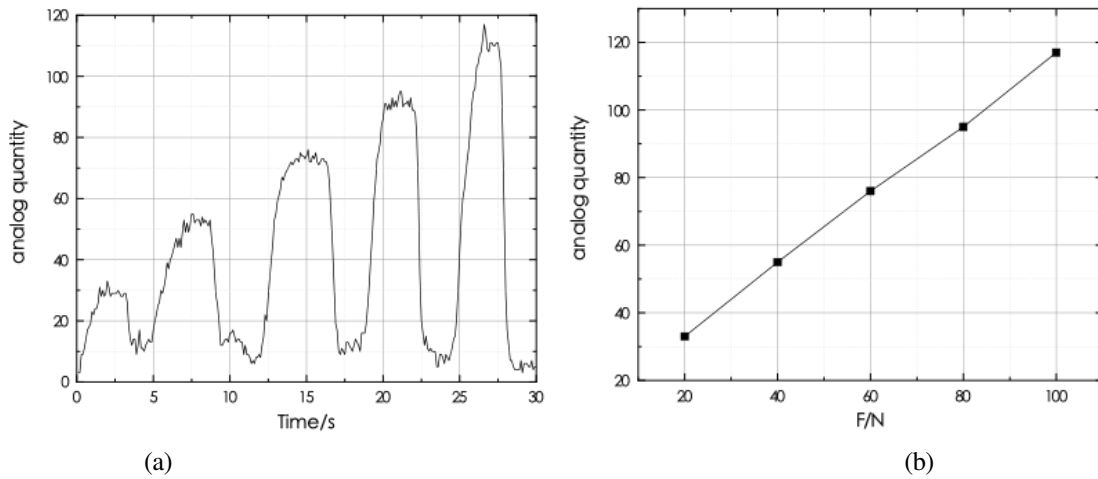


Figure 27: Line graphs determined from results (a) time vs analog quantity, (b) tensile force vs analog quantity

As seen from figure 27b, the graph is roughly linear meaning the analog quantity and tensile force are directly proportional, and the ratio is roughly 1.033. This is slightly off the actual value of $1023/1000 = 1.023$, with only an absolute difference of around 0.98%. Therefore, the hypothesis has been proven correct, and the tensile force x can be calculated as $x=y/1.023$ in which y is equal to the analog input.

Third experiment:

The third experiment investigates the relationship between the weight of the user while squatting and the analog value. As the second experiment determined a direct correlation between the analog value and tensile force, the analog value can be measured in this experiment to accurately obtain relevant data.

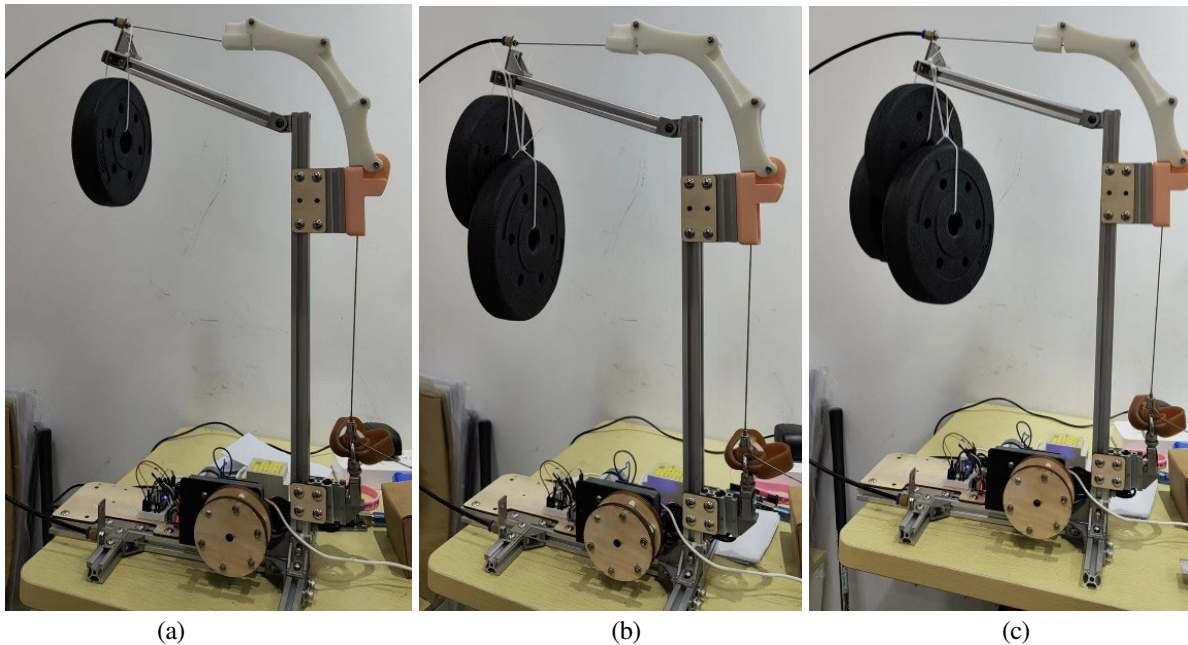


Figure 28: Experimental setup with weights attached to the system (a) 1.25kg, (b) 4kg, (c) 6kg

To set up the experiment, the system is placed on a flat table surface and the angle of the system is set at 109 degrees as shown in figure 28. 6 weights of 1.25kg, 1.5kg, 2kg, 2.5kg, 4kg, and 6kg are also placed on the edge of the metallic stand 24cm away from the center of motion, which is the knee joint (hinge).

During the experiment process, the changes in the analog quantity should be observed and recorded through the serial port monitor. As the value of the analog quantity is constantly fluctuating, data is collected every 0.1 seconds over a period of 100 seconds, resulting in a total of 1000 data points, thereby allowing for a more accurate model. After recording the data, the anomalies stemming from the irregular fluctuations are removed from the dataset and organized to determine an average analog quantity value.

Mass/KG	Average analog quantity before removed anomalies	Average analog quantity after removed anomalies
1.25	39.385	38.27607
1.5	58.853	57.20571
2	80.878	78.71056
2.5	114.226	112.3192
4	219.213	218.8242
6	439.222	436.901

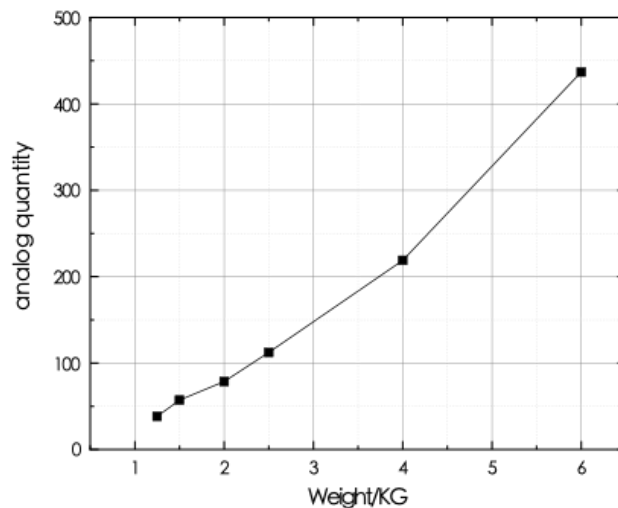


Figure 29: Line graph of weight vs analog quantity determined from results.

As seen from the line graph, there's also a direct correlation between the weight of the squatting user and the analog quantity, and the overall force required by the system can be predicted by the weight of the squatting user.

Fourth experiment:

The fourth experiment investigates the stability of the AI pose recognition system and if it is accurately able to assist the user during squatting motions. To set up this experiment, the computer will be placed on a flat surface 2 meters away from the user in which the user's right hip, knee, and ankle should all be in the frame. During the experiment, the user should gradually squat down and stand back up while observing and recording the analog quantity through the serial port monitor. From the experiments, it was observed that there weren't many irregular fluctuations in the analog quantity, meaning the overall tensile force is relatively stable and accurate. Therefore, it can be concluded that the pose recognition system is able to assist the user accurately and safely throughout their squatting motion.

Conclusion

This paper presents a semi-rigid exoskeleton that assists the user's overall knee joint performance and strength for those suffering from knee injuries or pains. The exoskeleton uses a routing structure and system to integrate the advantages of both rigid and soft exoskeleton systems, while directly addressing and negating most major concerns or downsides to the two systems such as misalignment and discomfort issues. In the future, a customizable system will be developed so that the users can determine the amount of assistive torque force they need to be applied to their knee joint depending on their current physical ability. This will allow for a more efficient recovery process for the user and maximize the potential for this exoskeleton.

References

- [1]. V. A. D. Cai, P. Bidaud, V. Hayward, F. Gosselin, and E. Desailly, "Self-adjusting, isostatic exoskeleton for the human knee joint," in Engineering in Medicine and Biology Society, EMBC, 2011 Annual International Conference of the IEEE, 2011, pp. 612-618.
- [2]. C. J. Walsh, K. Endo, and H. Herr, "A quasi-passive leg exoskeleton for load-carrying augmentation," *Int. J. Humanoid Robot.*, vol. 4, no. 3, pp. 487-506, 2007.
- [3]. Saccares, Lorenzo & Sarakoglou, Ioannis & Tsagarakis, Nikos. (2016). iT-Knee: An Exoskeleton with Ideal Torque Transmission Interface for Ergonomic Power Augmentation. 10.1109/IROS.2016.7759140.
- [4]. M. Wehner et al., "A lightweight soft exosuit for gait assistance," in Proc. IEEE Int. Conf. Robot. Automat., 2013, pp. 3362-3369.
- [5]. "Pose." Mediapipe, 2017, google.github.io/mediapipe/solutions/pose.html. Accessed 30 Nov.
- [6]. 2022. A. Kapandji, *The Physiology of the Joints: Lower Limb*, Volume 2, 5 ed.: Churchill Livingstone
- [7]. Lim JM, Cho JJ, Kim TY, Yoon BC. Isokinetic knee strength and proprioception before and after anterior cruciate ligament reconstruction: A comparison between home-based and supervised rehabilitation. *J Back Musculoskelet Rehabil.* 2019;32(3):421-429. doi: 10.3233/BMR-181237. PMID: 30507563.
- [8]. Dong-hai Wang, J. Guo, Kok-Meng Lee, Y. Can-jun, and H. Yu, "An adaptive knee joint exoskeleton based on biological geometries," in Proc. IEEE Int. Conf. Robot. Automat., 2011, pp. 1386-1391.
- [9]. H. Iwaki, V. Pinskerova, and M. Freeman, "Tibiofemoral movement 1: The shapes and relative movements of the femur and tibia in the unloaded ca- daver knee," *J. Bone Joint Surgery. Brit. vol.*, vol. 82, no. 8, pp. 1189-1195, 2000.

- [10]. Zoss, H. Kazerooni, and A. Chu, "On the mechanical design of the Berkeley lower extremity exoskeleton (BLEEX)," in Proc. IEEE/RSJ Int. Conf. Intell. Robots Syst., 2005, pp. 3465–3472.
- [11]. L. Saccares, A. Brygo, I. Sarakoglou, and N. G. Tsagarakis, "A novel human effort estimation method for knee assistive exoskeletons," in Proc. Int. Conf. Rehabil. Robot., 2017, pp. 1266–1272.
- [12]. S. H. Collins and A. Ruina, A bipedal walking robot with efficient and human-like gait, in IEEE Int. Conf. Robotics and Automation (ICRA) Barcelona, Spain (IEEE Press, 2005), pp. 1983–1988.
- [13]. V. T. Inman, H. J. Ralston and F. Todd, Kinetics of human locomotion, in Human Walking, ed. J. Rose and J. G. Gamble (Williams and Wilkins, Baltimore, 1981), p. 91.
- [14]. W. C. Flowers, A man-interactive simulator system for above-knee prosthetics studies, Ph.D. thesis, Massachusetts Institute of Technology (1972).
- [15]. Chu, H. Kazerooni and A. Zoss, On the biomimetic design of the Berkeley lower extremity exoskeleton (BLEEX), in IEEE Int. Conf. Robotics and Automation (ICRA) (IEEE Press, Barcelona, Spain, 2006), pp. 4356–4363.
- [16]. M. L. Palmer, Sagittal plane characterization of normal human ankle function across a range of walking gait speeds, M.S. thesis, Massachusetts Institute of Technology (2002).
- [17]. C. J. Walsh, K. Pasch and H. Herr, An autonomous, underactuated exoskeleton for
- [18]. load-carrying augmentation, in IEEE Int. Conf. Intelligent Robots and Systems (IROS) Beijing, China (IEEE Press, 2006), pp. 1410–1415.
- [19]. Dollar and H. Herr, "Lower extremity exoskeletons and active orthoses: Challenges and state-of-the-art," Robotics, IEEE Transactions on, vol. 24, no. 1, pp. 144–158, Feb. 2008.
- [20]. K. N. Gregorczyk, J. P. Obusek, L. Hasselquist, J. M. Schiffman, C. K. Bensek, D. Gutekunst and P. Frykman, The effects of a lower body exoskeleton load carriage assistive device on oxygen consumption and kinematics during walking with loads, in 25th Army Sci. Conf., Florida, USA (2006).
- [21]. A. Schiele, "Ergonomics of Exoskeletons: Objective Performance Metrics" in Euro Haptics conference on Haptic Interfaces, Salt Lake City, UT, USA, March 2009.
- [22]. Royer, T.D. and Martin, P.E (2005) 'Manipulations of Leg Mass and Moment of Inertia: Walking', Medicine & Science in Sports & Exercise, pp. 37(4): 649-656
- [23]. T. Nef and M. Mihelj and R. Riener, ARMin II – 7 DoF rehabilitation robot: mechanics and kinematics, 2007 IEEE International Conference on Robotics and Automation, 2007, pp. 4120-4125.
- [24]. A. Zoss, H. Kazerooni, and A. Chu, "On the mechanical design of the Berkeley Lower Extremity Exoskeleton (BLEEX)," in Intelligent Robots and Systems, 2005. (IROS 2005). 2005 IEEE/RSJ International Conference on, 2005, pp. 3465 -3472.
- [25]. A. H. A. Stienen, E. E. G. Hekman, F. C. T. v. d. Helm, and H. v. d. Kooij, "Self-Aligning Exoskeleton Axes Through Decoupling of Joint Rotations and Translations," IEEE Transactions on Robotics, vol. 25, pp. 628 - 633, 2009.
- [26]. E. S. G. a. J. W. Suntay, "A Joint Coordinate System for the Clinical Description of Three-Dimensional Motions: Application to the Knee," Journal of Biomechanics, vol. 105, 1983.
- [27]. I. A. Kapandji, The Physiology of the Joints: Lower Limb, Volume 2, 5 ed.: Churchill Livingstone
- [28]. N. C. Karavas, N. G. Tsagarakis, and D. G. Caldwell, "Design, modeling and control of a series elastic actuator for an assistive knee exoskeleton," in 2012 4th IEEE RAS & EMBS International Conference on Biomedical Robotics and Biomechatronics (BioRob), 2012, pp. 1813-1819.
- [29]. B. Celebi, M. Yalcin, and V. Patoglu, "AssistOn-Knee: A self-aligning knee exoskeleton," in Intelligent Robots and Systems (IROS), 2013 IEEE/RSJ International Conference on, 2013, pp. 996-1002.
- [30]. D. G. Caldwell, N. G. Tsagarakis, S. Kousidou, N. Costa, and I. Sarakoglou, ""SOFT" EXOSKELETONS FOR UPPER AND LOWER BODY REHABILITATION — DESIGN,
- [31]. CONTROL AND TESTING," International Journal of Humanoid Robotics, vol. 04, pp. 549-573, 2007/09/01 2007.

- [32]. R. W. Horst, "A bio -robotic leg orthosis for rehabilitation and mobility enhancement," in Engineering in Medicine and Biology Society, 2009. EMBC 2009. Annual International Conference of the IEEE, 2009, pp. 5030 -5033.
- [33]. H. Khan, R. Featherstone, D. G. Caldwell, and C. Semini, "Bio - inspired knee joint mechanism for a hydraulic quadruped robot," in Automation, Robotics and Applications (ICARA), 2015 6th International Conference on, 2015, pp. 325 -331.